Robotica (2016) volume 34, pp. 98–117. © Cambridge University Press 2014
doi:10.1017/S0263574714001350

Inverse kinematics solution of a new circumferential drilling machine for aircraft assembly

Weidong Zhu*, Biao Mei and Yinglin Ke

The State Key Lab of Fluid Power Transmission and Control, Department of Mechanical Engineering, Zhejiang University, Hangzhou 310027, China

(Accepted April 29, 2014. First published online: May 22, 2014)

SUMMARY

Inverse kinematics solutions are the basis for position and orientation control of automated machines in their Cartesian workspace. This paper presents an efficient and robust inverse kinematics algorithm for a new circumferential drilling machine for aircraft fuselage assembly. After a brief introduction to the circumferential drilling machine and its forward kinematics, the paper discusses the nonlinear optimization method for solving inverse kinematics problems. The objective function is defined as a weighted combination of a position error function and an orientation error function. By representing orientation error as the geodesic distance between two points on a unit sphere, the paper proposes to define the orientation error function by using faithful geodesic distance functions, which are accurate approximations to the geodesic distance when it is small. For increased efficiency, robustness, and easy setting of initial values, the inverse kinematics problem is decomposed into two subproblems. The revolute joint coordinates are obtained by nonlinear optimization, and the prismatic joint coordinates are calculated with closed-form formulas. Numerical experiments show that the objective function defined with faithful geodesic distance functions is effective, and the proposed algorithm is efficient, robust, and accurate. The algorithm has been successfully integrated into the control system of the circumferential drilling machine. Preliminary drilling experiments show that the position accuracy of drilled holes is within ±0.5 mm, which is acceptable for the assembly of large aircrafts.

KEYWORDS: Inverse kinematics; Nonlinear optimization; Orientation error function; Geodesic distance; Drilling machine; Aircraft assembly.

1. Introduction

In aircraft manufacturing, the fuselage of a large aircraft is assembled using several fuselage sections. In the assembly process, fuselage sections are first aligned with each other using numerical positioners,[1–2] then fastener holes are drilled in the circumferential splice region and adjacent sections are joined together using rivets or bolts. Due to the difficult-to-cut materials used in aircraft structures and high quality standard in aircraft manufacturing, the task of drilling fastener holes is labor intensive and costly. For improved efficiency, higher quality, and clean manufacturing, automated drilling machines must be employed in this task. Traditional gantry-type drilling machines require large investment, and furthermore, the deployment of these machines in the fuselage assembly station is often prevented by existing assembly fixtures. Therefore, an automated, low-cost, flexible, and small-size drilling machine is desirable for aircraft fuselage assembly. Electroimpact Inc. developed several flexible automated drilling machines based on the flex track technology, and successfully applied them to the manufacturing of the B777.[3–4] However, the cost of these machines is high (about $ 750, 000), and they are not suitable for drilling fastener holes on double-curved aircraft structures. To meet the challenges of low-cost and flexible drilling for aircraft fuselage assembly, a circumferential drilling machine was recently developed at Zhejiang University, which is shown in

* Corresponding author. E-mail: wdzhu@zju.edu.cn

Fig. 1. The circumferential drilling machine developed at Zhejiang University.

Fig. 1. The drilling machine has six numerical control axes and is suitable for drilling fastener holes on double-curved surfaces, e.g., the splice region of forward and central fuselage.

In the drilling process, the joint coordinates of the machine's axes must be determined in order to put the drilling tool at the correct position and orientation in the machine's Cartesian workspace. This problem is known as the inverse kinematics problem, which has been extensively studied in the robotics community for several decades.[5–11] For a serial-type machine, it is straightforward to compute the pose (position and orientation) in the Cartesian space when joint coordinates are given. However, the inverse kinematics problem requires the solution of nonlinear sets of equations. Closed-form and numerical solutions are two major categories of solutions for inverse kinematics problems. Closed-form solutions are desirable because they are exact and faster to compute, and all possible solutions can be identified when multiple solutions exist. However, closed-form solutions are only available for a few special kinematic structures,[12–17], e.g., when three consecutive revolute joint axes intersect at a common point or three consecutive revolute joint axes are parallel. Moreover, closed-form solutions are subject to uncertainty due to manufacturing errors.[18] Therefore, numerical algorithms are frequently employed to solve inverse kinematics problems. In the literature,[19–20] the Newton–Raphson method was used to solve the nonlinear kinematic equations. This method is unstable near singularities and cannot converge to exact singular configurations, and its stability strongly depends on the quality of the initial estimation of the solution. The damped Newton–Raphson methods, in which the Newton correction is modified using a damping factor λ, have been proposed to overcome these problems.[6,21–25] However, when the TCP (tool center point) is near the workspace boundary, these methods may generate solutions oscillating about the desired position. In addition to the Newton-Raphson methods, inverse kinematics problems have also been transformed into least-squares minimization problems and solved by nonlinear optimization algorithms.[21,26–28] Since the inverse Jacobian matrix is not used in these methods, they are numerically more stable than the Newton–Raphson methods. Typical nonlinear optimization methods such as the Levenberg–Marquardt method, steepest descent method, and variable metric method can be applied to solve minimization problems.[8,27,29–30] Among them, the Levenberg–Marquardt method is

https://doi.org/10.1017/S0263574714001350 Published online by Cambridge University Press

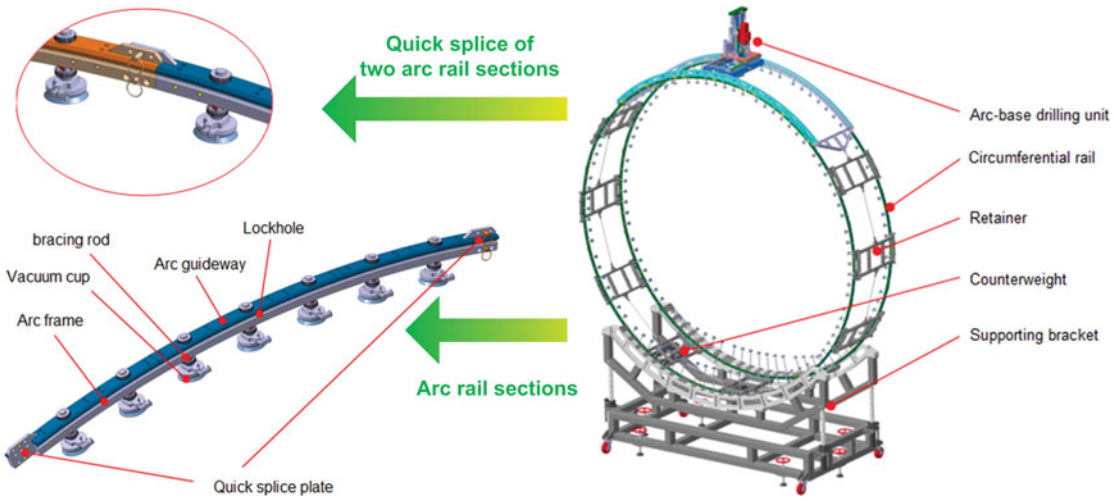

Fig. 2. Structure of the circumferential drilling machine.

more preferable because of its high stability and satisfactory convergence performance in numerical optimization.[31]

Although methods based on numerical optimization are quite general for solving inverse kinematics problems, there is still no general method that is efficient and robust for all kinematic structures. The complexity of the minimization problem is highly dependent on the formulation of the objective function,[26] and it has been shown in literature that the combination of closed-form solutions of partial kinematic chains with numerical algorithms is advantageous for robustness and efficiency in solving inverse kinematics problems.[6,32–33] In this paper, for increased robustness, efficiency, and easy assignment of initial values, the inverse kinematics problem of the circumferential drilling machine is decomposed into two subproblems by exploring the characteristics of the machine's kinematic structure. The revolute joint coordinates are found using nonlinear optimization, and the prismatic joint coordinates are computed with closed-form formulas. The objective function to be minimized in solving the inverse kinematics problem is typically composed of a position error function and an orientation error function. While the Euclidean distance has been commonly used in formulating the position error function of two points, there is no such common view in formulating the orientation error function of two vectors. Various orientation error functions have been proposed in literature,[8,27–28,31,34] however, there still lacks a suitable method to analyze their performance. In this paper, the orientation error function is deduced from a geometric point of view. By representing the orientation error as the geodesic distance between two points on a unit sphere, the paper proposes to use faithful geodesic distance functions to formulate the orientation error function. Furthermore, the concept of faithful geodesic distance can be used to predict the performance of different orientation error functions proposed in literature.

This paper is organized as follows: Section 2 discusses the forward kinematics model after a brief introduction to the circumferential drilling machine. Section 3 discusses the framework to solve the inverse kinematics problem with nonlinear optimization methods. Section 4 discusses the representation of orientation errors as geodesic distances on the unit sphere, the definition of faithful geodesic distance functions, and the formulation of orientation error function with faithful geodesic distance functions. Section 5 presents the method to decompose the original inverse kinematics problem into two subproblems. Section 6 describes the numerical experiments in detail, including the weighting methods, initial values, convergence criteria, experimental procedure, and the analysis of the results. Preliminary drilling experiments with the circumferential drilling machine are also discussed. Finally, conclusions are drawn in Section 7.

2. Kinematic Model of the Circumferential Drilling System

The circumferential drilling machine mainly consists of a supporting bracket, two circumferential rails, and an arc-base drilling unit, as shown in Fig. 2.

https://doi.org/10.1017/S0263574714001350 Published online by Cambridge University Press

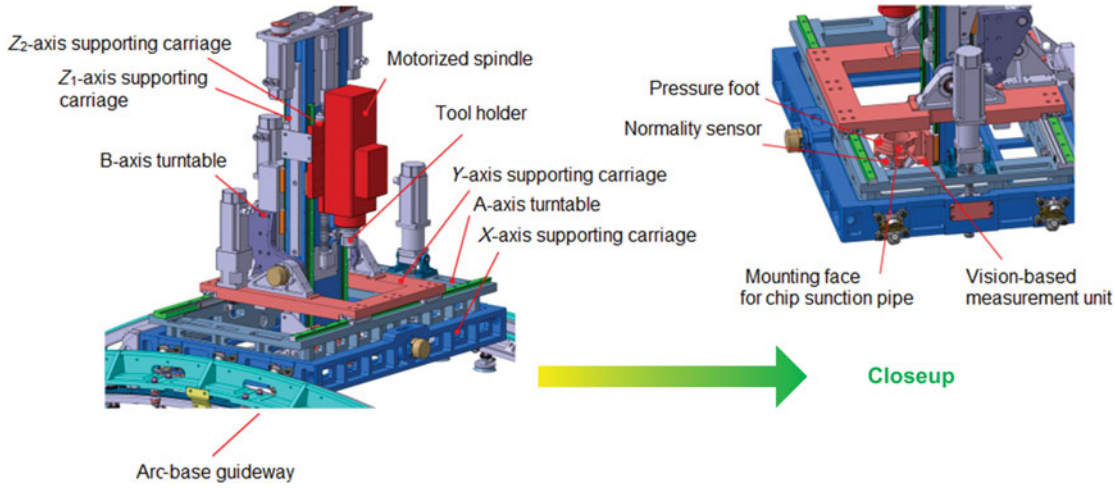

Fig. 3. The arc-base drilling unit.

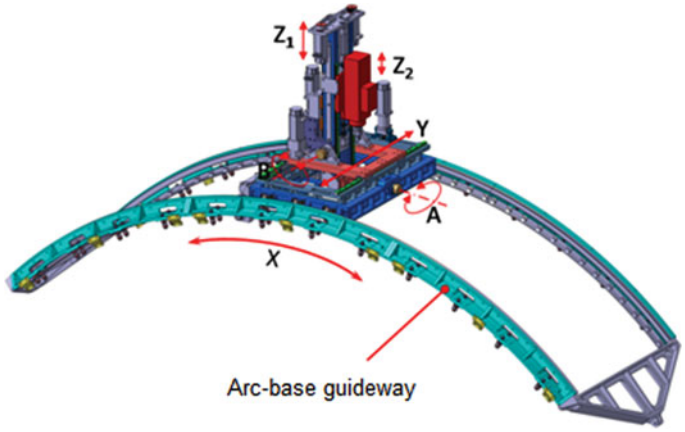

Fig. 4. Numerically controlled motion axes of arc-base drilling unit.

The supporting bracket is used to partially support the weight of the circumferential drilling machine for better stability and safety in drilling. Both circumferential rails are attached to the aircraft structure with vacuum cups, forming a solid structure for mounting the arc-base drilling unit. Before drilling, the arc-base drilling unit is moved to the targeted region and fixed to the circumferential rails by the operator. Then, the arc-base drilling unit can perform automated drilling within the span of an arc. The arc-base drilling unit consists of an arc base, **X**-, **Y**-, $\mathbf{Z}_1$-, and $\mathbf{Z}_2$-axis supporting carriages, **A**- and **B**-axis turntables, a tool holder, a pressure foot, a normality sensing unit, and a vision unit (refer to Fig. 3). The pressure foot is used to eliminate the gap between the stacks of the aircraft structure, and keep the drilling process stable. The normality sensing unit measures the orientation error of the drill and provides feedback information for controlling the drill so that it is perpendicular to the workpiece surface before drilling. The vision unit detects reference holes online for calibrating base frame position of the arc-base drilling unit with respect to the aircraft structure. Thus, the position accuracy of the drilled fastener holes is largely determined by the positioning accuracy of the arc-base drilling unit.

The arc-base drilling unit has six numerically controlled motion axes, as shown in Fig. 4, in which the **X**- and **Y**-axis use rack and pinion transmissions and other axes use ball screw and nut transmissions. The **X**- and **Y**-axis are used to position the drill along circumferential and longitudinal directions, respectively. The rotational **A**- and **B**-axis are controlled coordinately to achieve the normality of the drill relative to the surface of the aircraft structure. The $\mathbf{Z}_1$- and $\mathbf{Z}_2$-axis are two parallel linear axes along the drilling direction. They are designed for different purposes: the $\mathbf{Z}_1$-axis with larger motion range is mainly for obstacle avoidance, providing space for tool exchange, and

https://doi.org/10.1017/S0263574714001350 Published online by Cambridge University Press

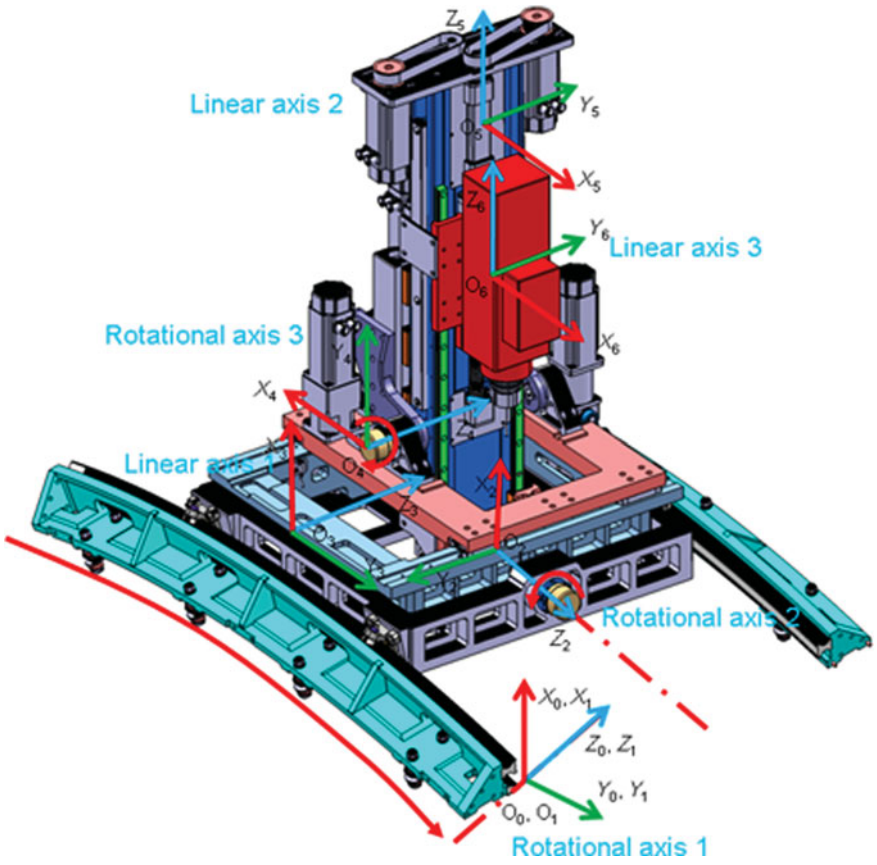

Fig. 5. Kinematic structure of the arc-base drilling unit.

adapting to the curvature of aircraft structures, while the $\mathbf{Z}_2$-axis provides feed motion along the drilling direction.

All axes use conventional mechanism to realize prismatic (linear guideway/bearing) or revolute (shaft/bearing) joints except the **X**-axis of the drilling unit, which uses an arc-shaped guideway and offers motion along a circular trajectory. Consequently, the **X**-axis is modeled as a revolute joint. The arc length traveled along the arc-shaped guideway is related to the rotation angle by $\theta_1 = L/R$, where L is the arc length along the arc-shaped guideway, and R is the radius of the motion trajectory. The parameter R is an internal modeling parameter for the revolute joint and is measured to be 2425.02 mm.

In kinematic modeling, the six joints of the arc-base drilling unit are denoted as $joint_i, i = 1, 2, \ldots, 6$, where $joint_i$ generates motion between $link_{i-1}$ and $link_i$. And the links are numbered from 0 to 6 starting from the arc base, which is denoted as $link_0$. Each link is attached with a proper coordinate frame so that the pose (position and orientation) of the link with respect to its adjacent link(s) can be described mathematically, e.g., $link_i$ is assigned with frame $\{O_i X_i Y_i Z_i\}$ (refer to Fig. 5). When assigning a right-hand orthogonal coordinate frame to a link, the Z-axis, origin, and X-axis are determined according to the geometric configurations of the machine, while the Y-axis is determined with the right-hand rule. The Z-axis of frame $\{O_i X_i Y_i Z_i\}$ assigned to $link_i$ coincides with the motion direction of $joint_i$. Frame $\{O_i X_i Y_i Z_i\}$ is determined according to the D–H (Denavit–Hartenberg) method when the common perpendicular between adjacent axes can be determined uniquely; otherwise, it is determined using a modified version of the Hayati method,[35] in which the origin is defined by intersecting $joint_i$ with a coordinate plane (XYor XZ) of frame $\{O_{i-1} X_{i-1} Y_{i-1} Z_{i-1}\}$. The kinematic model of the arc-base drilling unit is constructed using a sequence of homogeneous transformation matrices from its base frame to the TCP frame. The determination of link frames and transformation matrices between adjacent links are discussed as follows:

(1) Frame $\{O_0 X_0 Y_0 Z_0\}$ and 2) Frame $\{O_1 X_1 Y_1 Z_1\}$.

https://doi.org/10.1017/S0263574714001350 Published online by Cambridge University Press

The base frame $\{O_0X_0Y_0Z_0\}$ is defined to be coincident with frame $\{O_1X_1Y_1Z_1\}$ when $joint_1$ is at zero position. $joint_1$ and $joint_2$ are revolute joints perpendicular to each other, frame $\{O_1X_1Y_1Z_1\}$ can be determined unambiguously using the D–H method. Its Z-axis is chosen along the positive direction of $joint_1$, its origin is placed at the intersection of $joint_1$ and the common perpendicular between $joint_1$ and $joint_2$, and its X-axis is chosen along the common perpendicular, pointing from $joint_1$ to $joint_2$. The pose of frame $\{O_1X_1Y_1Z_1\}$ with respect to the base frame is

$$T_{01} = R_z(\theta_1) = \begin{bmatrix} C\theta_1 & -S\theta_1 & 0 & 0 \\ S\theta_1 & C\theta_1 & 0 & 0 \\ 0 & 0 & 1 & 0 \\ 0 & 0 & 0 & 1 \end{bmatrix}, \tag{1}$$

where θ_1 is the rotation angle of $joint_1$.

(3) Frame $\{O_2X_2Y_2Z_2\}$

The origin of $\{O_2X_2Y_2Z_2\}$ is defined as the intersection of $joint_2$ and the common perpendicular between $joint_1$ and $joint_2$. The Z-axis of $\{O_2X_2Y_2Z_2\}$ is defined along the positive direction of $joint_2$, and the X-axis of $\{O_2X_2Y_2Z_2\}$ is defined to be parallel to the X-axis of frame $\{O_1X_1Y_1Z_1\}$ when $joint_2$ is at zero position. The pose of frame $\{O_2X_2Y_2Z_2\}$ with respect to frame $\{O_1X_1Y_1Z_1\}$ is

$$T_{12} = T_x(a_2)R_x(-90^\circ)R_x(\alpha_2)R_z(\theta_2) = \begin{bmatrix} C\theta_2 & -S\theta_2 & 0 & a_2 \\ S\alpha_2S\theta_2 & S\alpha_2C\theta_2 & C\alpha_2 & 0 \\ -C\alpha_2S\theta_2 & -C\alpha_2C\theta_2 & S\alpha_2 & 0 \\ 0 & 0 & 0 & 1 \end{bmatrix}, \tag{2}$$

where θ_2 is the rotation angle of $joint_2$, a_2 is the length of the common perpendicular between $joint_1$ and $joint_2$, $\alpha_2 - 90^\circ$ is the angle between the Z-axes of frame $\{O_1X_1Y_1Z_1\}$ and frame $\{O_2X_2Y_2Z_2\}$.

(4) Frame $\{O_3X_3Y_3Z_3\}$

The prismatic $joint_3$ is defined as a line intersecting the XZ plane of frame $\{O_2X_2Y_2Z_2\}$ at $(c_{31}, 0, c_{32})$, where c_{31}, c_{32} are arbitrary constants. Then, by applying rules similar to the Hayati method, frame $\{O_3X_3Y_3Z_3\}$ can be obtained by the following steps:

a) Translate the origin of frame $\{O_2X_2Y_2Z_2\}$ to $(c_{31}, 0, c_{32})$;
b) Rotate the resulting frame around its X-axis by 90° so that its Z-axis is nominally aligned with the Z-axis of $\{O_3X_3Y_3Z_3\}$;
c) Rotate the resulting frame around its X-axis by α_3, then rotate the resulting frame around its Y-axis by β_3 to align with frame $\{O_3X_3Y_3Z_3\}$ when $joint_3$ is at zero position;
d) Translate the resulting frame along its Z-axis by d to acquire frame $\{O_3X_3Y_3Z_3\}$, where d is the displacement of $joint_3$.

Thus, the pose of frame $\{O_3X_3Y_3Z_3\}$ with respect to frame $\{O_2X_2Y_2Z_2\}$ is

$$\begin{aligned} T_{23} &= T_x(c_{31})T_z(c_{32})R_x(90^\circ)R_x(\alpha_3)R_y(\beta_3)T_z(d_3) \\ &= \begin{bmatrix} C\beta_3 & 0 & S\beta_3 & c_{31} + d_3S\beta_3 \\ C\alpha_3S\beta_3 & -S\alpha_3 & -C\alpha_3C\beta_3 & -d_3C\alpha_3C\beta_3 \\ S\alpha_3S\beta_3 & C\alpha_3 & -S\alpha_3C\beta_3 & c_{32} - d_3S\alpha_3C\beta_3 \\ 0 & 0 & 0 & 1 \end{bmatrix}. \end{aligned} \tag{3}$$

(5) Frame $\{O_4X_4Y_4Z_4\}$

The revolute $joint_4$ is nominally parallel to the prismatic $joint_3$. Frame $\{O_4X_4Y_4Z_4\}$ is determined as follows:

https://doi.org/10.1017/S0263574714001350 Published online by Cambridge University Press

a) Place the origin of the $\{O_4X_4Y_4Z_4\}$ at the intersection of $joint_4$ and the XY plane of $\{O_3X_3Y_3Z_3\}$. This is achieved by translating $\{O_3X_3Y_3Z_3\}$ along its X- and Y-axis by a_4 and d_4, respectively;
b) Rotate the resulting frame around Z-axis by -90° so that the resulting X-axis points from $joint_4$ to $joint_5$;
c) Rotate the resulting frame around X-axis by α_4 and Y-axis by β_4 to align the Z-axis with that of frame $\{O_4X_4Y_4Z_4\}$;
d) Finally, rotate around the Z-axis by θ_4 to obtain frame $\{O_4X_4Y_4Z_4\}$.

Hence, the pose of frame $\{O_4X_4Y_4Z_4\}$ with respect to $\{O_3X_3Y_3Z_3\}$ is

$$T_{34} = T_x(a_4)T_y(d_4)R_z(-90^\circ)R_x(\alpha_4)R_y(\beta_4)R_z(\theta_4) = \begin{bmatrix} C\alpha_4S\theta_4 + S\alpha_4S\beta_4C\theta_4 & C\alpha_4C\theta_4 - S\alpha_4S\beta_4S\theta_4 & -S\alpha_4C\beta_4 & a_4 \\ -C\beta_4C\theta_4 & C\beta_4S\theta_4 & -S\beta_4 & d_4 \\ S\alpha_4S\theta_4 - C\alpha_4S\beta_4C\theta_4 & S\alpha_4C\theta_4 + C\alpha_4S\beta_4S\theta_4 & C\alpha_4C\beta_4 & 0 \\ 0 & 0 & 0 & 1 \end{bmatrix}. \quad (4)$$

(6) Frame $\{O_5X_5Y_5Z_5\}$

$joint_5$ is a prismatic joint and is defined as a line intersecting the XZ plane of $\{O_4X_4Y_4Z_4\}$ at $(c_{51}, 0, c_{52})$, where c_{51}, c_{52} are arbitrary constants. Frame $\{O_5X_5Y_5Z_5\}$ can be acquired as follows:

a) Translate $\{O_4X_4Y_4Z_4\}$ along the X-axis and Z-axis by c_{51} and c_{52}, respectively;
b) Rotate around the Z-axis by 180° so that the resulting X-axis nominally points in the direction from $joint_5$ to $joint_6$;
c) Rotate around the resulting X-axis to nominally align the Z-axis with the positive direction of $joint_5$;
d) Rotate around the X- and Y-axis by α_5 and β_5, respectively, to align its Z-axis with the positive direction of $joint_5$;
e) Translate along the Z-axis by d_5 to acquire frame $\{O_5X_5Y_5Z_5\}$.

The pose of frame $\{O_5X_5Y_5Z_5\}$ with respect to $\{O_4X_4Y_4Z_4\}$ is

$$T_{45} = T_x(c_{51})T_z(c_{52})R_z(180^\circ)R_x(90^\circ)R_x(\alpha_5)R_y(\beta_5)T_z(d_5) = \begin{bmatrix} -C\beta_5 & 0 & -S\beta_5 & c_{51} - d_5S\beta_5 \\ -C\alpha_5S\beta_5 & S\alpha_5 & C\alpha_5C\beta_5 & d_5C\alpha_5C\beta_5 \\ S\alpha_5S\beta_5 & C\alpha_5 & -S\alpha_5C\beta_5 & c_{52} - d_5S\alpha_5C\beta_5 \\ 0 & 0 & 0 & 1 \end{bmatrix}. \quad (5)$$

(7) Frame $\{O_6X_6Y_6Z_6\}$

$joint_6$ is a prismatic joint, which is defined as a line intersecting the XY plane of $\{O_5X_5Y_5Z_5\}$ at $(c_{61}, c_{62}, 0)$, where c_{61}, c_{62} are arbitrary constants. Frame $\{O_6X_6Y_6Z_6\}$ is determined in the same way as frame $\{O_5X_5Y_5Z_5\}$ as follows:

a) Translate frame $\{O_5X_5Y_5Z_5\}$ along the X-axis and Y-axis by c_{61} and c_{62}, respectively.
b) Rotate around the X-axis and Y-axis to align the Z-axis with $joint_6$
c) Translate along the Z-axis by d_6 to represent the linear motion along $joint_6$

The pose of frame $\{O_6X_6Y_6Z_6\}$ with respect to frame $\{O_5X_5Y_5Z_5\}$ is

$$T_{56} = T_x(c_{61})T_y(c_{62})R_x(\alpha_6)R_y(\beta_6)T_z(d_6) = \begin{bmatrix} C\beta_6 & 0 & S\beta_6 & c_{61} + d_6S\beta_6 \\ S\alpha_6S\beta_6 & C\alpha_6 & -S\alpha_6C\beta_6 & c_{62} - d_6S\alpha_6C\beta_6 \\ -C\alpha_6S\beta_6 & S\alpha_6 & C\alpha_6C\beta_6 & d_6C\alpha_6C\beta_6 \\ 0 & 0 & 0 & 1 \end{bmatrix}. \quad (6)$$

https://doi.org/10.1017/S0263574714001350 Published online by Cambridge University Press

(8) TCP frame

Since the drilling tool axis is parallel to $joint_6$, the TCP is defined as a translated frame of $\{O_6X_6Y_6Z_6\}$ along three coordinate axes as follows:

$$T_{67} = T_x(x_7)T_y(y_7)T_z(z_7) = \begin{bmatrix} 1 & 0 & 0 & x_7 \\ 0 & 1 & 0 & y_7 \\ 0 & 0 & 1 & z_7 \\ 0 & 0 & 0 & 1 \end{bmatrix}, \tag{7}$$

where x_7, y_7, z_7 are translations along the X-, Y- and Z-axis, respectively.

After assigning a coordinate frame to each link, a forward kinematic model of the 6-DOF arc-base drilling unit is formulated as

$$T_{07} = T_{01}T_{12}T_{23}T_{34}T_{45}T_{56}T_{67}, \tag{8}$$

where $\mathbf{q} = [\theta_1, \theta_2, d_3, \theta_4, d_5, d_6]$ are joint variables, $\mathbf{p} = [a_2, \alpha_2, \alpha_3, \beta_3, a_4, d_4, \alpha_4, \beta_4, \alpha_5, \beta_5, \alpha_6, \beta_6, x_7, y_7, z_7]$ are kinematic parameters, and $\mathbf{c} = [c_{31}, c_{32}, c_{51}, c_{52}, c_{61}, c_{62}]$ are arbitrary constants used in the modeling of prismatic joints $joint_3$, $joint_5$, and $joint_6$.

3. Inverse Kinematics Solution Based on Nonlinear Minimization

For a serial-type machine, the forward kinematics can be represented by the following equation:

$$T(\mathbf{q}) = \begin{bmatrix} r_{11}(\mathbf{q}) & r_{12}(\mathbf{q}) & r_{13}(\mathbf{q}) & p_x(\mathbf{q}) \\ r_{21}(\mathbf{q}) & r_{22}(\mathbf{q}) & r_{23}(\mathbf{q}) & p_y(\mathbf{q}) \\ r_{31}(\mathbf{q}) & r_{32}(\mathbf{q}) & r_{33}(\mathbf{q}) & p_z(\mathbf{q}) \\ 0 & 0 & 0 & 1 \end{bmatrix}, \tag{9}$$

where $\mathbf{q} = [q_1, q_2, \ldots, q_n]$ is the vector of joint variables, and $T(\mathbf{q})$ is the homogeneous transformation matrix representing the position and orientation of TCP with respect to the machine base frame.

The inverse kinematics problem is to find the corresponding set of joint coordinates for the desired TCP pose with respect to the base frame,

$$T_d = \begin{bmatrix} u_x & v_x & w_x & o_x \\ u_y & v_y & w_y & o_y \\ u_z & v_z & w_z & o_z \\ 0 & 0 & 0 & 1 \end{bmatrix}. \tag{10}$$

This problem can be formulated as a matrix equation

$$T(\mathbf{q}) = T_d, \tag{11}$$

which yields 12 nontrivial scalar equations in the unknown variables $\mathbf{q}$. As discussed in Section 1, this set of nonlinear equations can be solved with iterative numerical algorithms, e.g., the Newton–Raphson method. For better numerical stability and robustness,[31] this root finding problem can be transformed into a minimization problem

$$J(\mathbf{q}) = \omega_1 J_{pos}(\mathbf{q}) + \omega_2 J_{ori}(\mathbf{q}) \rightarrow \min, \tag{12}$$

where $J_{pos}(\mathbf{q})$ is a scalar function reflecting the position errors between the current origin $[p_x(\mathbf{q}), p_y(\mathbf{q}), p_z(\mathbf{q})]^T$ and the desired origin $[o_x, o_y, o_z]^T$ of the TCP; $J_{ori}(\mathbf{q})$ is a scalar function reflecting the orientation errors between the current coordinate axes $[r_{11}(\mathbf{q}), r_{21}(\mathbf{q}), r_{31}(\mathbf{q})]^T$, $[r_{12}(\mathbf{q}), r_{22}(\mathbf{q}), r_{32}(\mathbf{q})]^T$, $[r_{13}(\mathbf{q}), r_{23}(\mathbf{q}), r_{33}(\mathbf{q})]^T$ and the desired coordinate axes $[u_x, u_y, u_z]$, $[v_x, v_y, v_z]$, $[w_x, w_y, w_z]$; and ω_1, ω_2 are weights balancing position errors and orientation errors.

https://doi.org/10.1017/S0263574714001350 Published online by Cambridge University Press

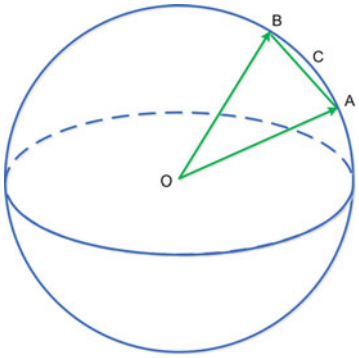

Fig. 6. Presentation of orientation error by faithful geodesic distance.

Functions $J_{pos}(\mathbf{q})$ and $J_{ori}(\mathbf{q})$ are nonnegative functions that attain their minimum values at joint coordinates $\mathbf{q}*$ satisfying Eq. (11). The detailed definitions of these functions are postponed to later sections.

4. Formulation of the Orientation Error Function

Let $V_1 = [x_1, y_1, z_1]^T$ and $V_2 = [x_2, y_2, z_2]^T$ be two unit vectors, then the orientation error between them can be defined as the subtended angle of the two vectors,

$$\varepsilon = \arccos(V_1 \cdot V_2). \tag{13}$$

However, this definition does not lead to an efficient orientation error function for solving the inverse kinematics problem. In this paper, we investigate the orientation error between two vectors from the geometric point of view.

Let's represent V_1 and V_2 as points A and B on the unit sphere, respectively (refer to Fig. 6). Thus, the orientation error between two vectors can be defined as the geodesic distance between the corresponding points on the unit sphere, which is the length of arc ACB of the great circle passing through points A and B.

Let δ denote the Euclidean distance between points A and B

$$\delta = \|V_1 - V_2\| = \sqrt{(x_1 - x_2)^2 + (y_1 - y_2)^2 + (z_1 - z_2)^2}. \tag{14}$$

It can be seen that δ is a function of the geodesic distance s between A and B on the unit sphere

$$\delta = 2\sin(s/2) \approx s - s^3/24 + s^5/1920. \tag{15}$$

In the inverse kinematics problem, s is a small value when reasonable initial values of the joint coordinates are provided, and it gets smaller and smaller as the nonlinear optimization algorithm iterates. Hence, higher order terms in Eq. (15) can be neglected, and the geodesic distance s can be faithfully represented by

$$s_F = \delta = \sqrt{(x_1 - x_2)^2 + (y_1 - y_2)^2 + (z_1 - z_2)^2} \tag{16}$$

In this paper, the function s_F is called a faithful geodesic distance function. It satisfies two properties:

Property 1: s_F is zero if and only if s is zero;

Property 2: $\frac{ds_F}{ds}|_{s=0} = \lim_{s->0} \frac{s_F}{s} = 1$, i.e., the first-order approximation to s_F is equal to s.

In literature,[8,34] the function $h = 1 - V_1 \cdot V_2$ was used to formulate the orientation error function. When geometrically represented (refer to Fig. 7), h is the length of the line segment BD, its relationship

https://doi.org/10.1017/S0263574714001350 Published online by Cambridge University Press

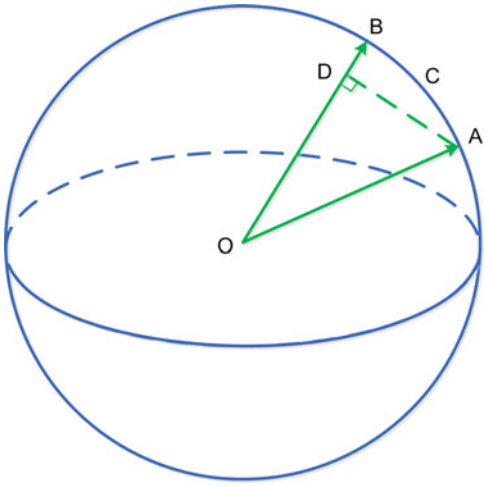

Fig. 7. Presentation of orientation error in refs. [8, 34] (a) $\omega_1 = \omega_2 = 1$; (b) $\omega_1 = (180/\pi)^2$, $\omega_2 = 1$.

with the geodesic distance s between A and B is

$$h = 1 - \cos(s) \approx s^2/2 - s^4/24. \tag{17}$$

The function h satisfies Property 1, but does not satisfy Property 2. Hence, from the viewpoint of this paper, it is not a faithful geodesic distance function and should not be used to formulate the orientation error function. This statement is confirmed by numerical experiments discussed in Section 6.

5. Decomposition of the Inverse Kinematic Problem

In the kinematic modeling stage, coordinate frames for prismatic joints are defined according to their physical positions in order to be intuitive, and arbitrary constants are introduced in the forward kinematic model. However, the arbitrary constants $\mathbf{c} = [c_{31}, c_{32}, c_{51}, c_{52}, c_{61}, c_{62}]$ do not actually affect the kinematic relationship, and are set to zero for computational efficiency.

The inverse kinematics problem of the nominal kinematic model is first studied, where parameters $a_2, a_4, d_4, x_7, y_7, z_7$ are nonzero values, and parameters $\alpha_2, \alpha_3, \beta_3, \alpha_4, \beta_4, \alpha_5, \beta_5, \alpha_6, \beta_6$ are zero values. The solution to the nominal kinematics can be used as good initial values for solving the inverse kinematics problem when manufacturing and assembly errors of machine need to be considered.

The nominal kinematic model is represented as follows:

$$T_{07}(\theta_1, \theta_2, d_3, \theta_4, d_5, d_6) = \begin{bmatrix} C\theta_4 S\theta_1 + C\theta_1 C\theta_2 S\theta_4 & -C\theta_1 S\theta_2 & C\theta_1 C\theta_2 C\theta_4 - S\theta_1 S\theta_4 & p_x \\ C\theta_1 C\theta_4 - C\theta_2 S\theta_1 S\theta_4 & S\theta_1 S\theta_2 & -C\theta_1 S\theta_4 - C\theta_2 C\theta_4 S\theta_1 & p_y \\ S\theta_2 S\theta_4 & C\theta_2 & C\theta_4 S\theta_2 & p_z \\ 0 & 0 & 0 & 1 \end{bmatrix}, \tag{18}$$

where $S(\bullet)$ and $C(\bullet)$ are sine and cosine functions, respectively, $\theta_1, \theta_2, d_3, \theta_4, d_5, d_6$ are joint variables, and p_x, p_y, p_z are

$$\begin{aligned} p_x = {} & (d_6 - d_5)(S\theta_1 S\theta_4 - C\theta_1 C\theta_2 C\theta_4) + x_7(C\theta_4 S\theta_1 + C\theta_1 C\theta_2 S\theta_4) - z_7(S\theta_1 S\theta_4 - C\theta_1 C\theta_2 C\theta_4) \\ & + a_2 C\theta_1 + d_4 S\theta_1 + a_4 C\theta_1 C\theta_2 + d_3 C\theta_1 S\theta_2 - y_7 C\theta_1 S\theta_2, \end{aligned} \tag{19}$$

$$\begin{aligned} p_y = {} & (d_6 - d_5)(C\theta_1 S\theta_4 + C\theta_2 C\theta_4 S\theta_1) + x_7(C\theta_1 C\theta_4 - C\theta_2 S\theta_1 S\theta_4) \\ & - z_7(C\theta_1 S\theta_4 + C\theta_2 C\theta_4 S\theta_1) + d_4 C\theta_1 - a_2 S\theta_1 - a_4 C\theta_2 S\theta_1 - d_3 S\theta_1 S\theta_2 + y_7 S\theta_1 S\theta_2, \end{aligned} \tag{20}$$

$$p_z = y_7 C\theta_2 - d_3 C\theta_2 + a_4 S\theta_2 - (d_6 - d_5) C\theta_4 S\theta_2 + z_7 C\theta_4 S\theta_2 + x_7 S\theta_2 S\theta_4. \tag{21}$$

https://doi.org/10.1017/S0263574714001350 Published online by Cambridge University Press

In the inverse kinematics for drilling, the corresponding joint coordinates should be determined for desired position $[o_x, o_y, o_z]^T$ and orientation $[w_x, w_y, w_z]^T$ of the hole axis.

From Eqs. (18)–(21), it can be observed that prismatic variables d_3, d_5, d_6 do not affect the orientation of the TCP. Hence, their coordinates should be determined from the position Eqs. (19)–(21), which are represented in matrix form as follows:

$$A \begin{bmatrix} d_3 \\ d_5 \\ d_6 \end{bmatrix} = \begin{bmatrix} b_1 \\ b_2 \\ b_3 \end{bmatrix}, \tag{22}$$

where

$$A = \begin{bmatrix} C\theta_1 S\theta_2 & -S\theta_1 S\theta_4 + C\theta_1 C\theta_2 C\theta_4 & S\theta_1 S\theta_4 - C\theta_1 C\theta_2 C\theta_4 \\ -S\theta_1 S\theta_2 & -C\theta_1 S\theta_4 - C\theta_2 C\theta_4 S\theta_1 & C\theta_1 S\theta_4 + C\theta_2 C\theta_4 S\theta_1 \\ -C\theta_2 & C\theta_4 S\theta_2 & -C\theta_4 S\theta_2 \end{bmatrix},$$

$$\begin{aligned} b_1 &= o_x - x_7(C\theta_4 S\theta_1 + C\theta_1 C\theta_2 S\theta_4) + z_7(S\theta_1 S\theta_4 - C\theta_1 C\theta_2 C\theta_4) - a_2 C\theta_1 - d_4 S\theta_1 - a_4 C\theta_1 C\theta_2 \\ &\quad + y_7 C\theta_1 S\theta_2, \\ b_2 &= o_y - x_7(C\theta_1 C\theta_4 - C\theta_2 S\theta_1 S\theta_4) + z_7(C\theta_1 S\theta_4 + C\theta_2 C\theta_4 S\theta_1) - d_4 C\theta_1 + a_2 S\theta_1 + a_4 C\theta_2 S\theta_1 \\ &\quad - y_7 S\theta_1 S\theta_2, \\ b_3 &= o_z - y_7 C\theta_2 - a_4 S\theta_2 - z_7 C\theta_4 S\theta_2 - x_7 S\theta_2 S\theta_4. \end{aligned}$$

It can be observed that the second and third columns of matrix A are dependent, i.e., $rank(A) = 2$. Hence, only variable d_3 and the difference of d_5 and d_6 can be determined from Eq. (22). This can be explained from the fact that $joint_5$ and $joint_6$ are two prismatic joints parallel to each other, which only provide one degree of motion freedom in the Cartesian space.

From Eqs. (19) and (21), d_3 and $d_6 - d_5$ can be obtained as follows:

$$\begin{aligned} d_3 &= -(x_7 S\theta_1 S\theta_2 - o_x C\theta_4 S\theta_2 - y_7 C\theta_1 C\theta_4 - o_z S\theta_1 S\theta_4 + o_z C\theta_1 C\theta_2 C\theta_4 + a_2 C\theta_1 C\theta_4 S\theta_2 \\ &\quad + d_4 C\theta_4 S\theta_1 S\theta_2 + y_7 C\theta_2 S\theta_1 S\theta_4 + a_4 S\theta_1 S\theta_2 S\theta_4)/(C\theta_1 C\theta_4 - C\theta_2 S\theta_1 S\theta_4), \end{aligned} \tag{23}$$

$$\begin{aligned} d_6 - d_5 &= (a_4 C\theta_1 - o_x C\theta_2 + a_2 C\theta_1 C\theta_2 + z_7 C\theta_1 C\theta_4 + d_4 C\theta_2 S\theta_1 + x_7 C\theta_1 S\theta_4 \\ &\quad - o_z C\theta_1 S\theta_2 + x_7 C\theta_2 C\theta_4 S\theta_1 - z_7 C\theta_2 S\theta_1 S\theta_4)(C\theta_1 C\theta_4 - C\theta_2 S\theta_1 S\theta_4). \end{aligned} \tag{24}$$

Referring to Eqs. (19)–(21), component position error can be defined as

$$\begin{aligned} E_x &= (d_6 - d_5)(S\theta_1 S\theta_4 - C\theta_1 C\theta_2 C\theta_4) + x_7(C\theta_4 S\theta_1 + C\theta_1 C\theta_2 S\theta_4) - z_7(S\theta_1 S\theta_4 - C\theta_1 C\theta_2 C\theta_4) \\ &\quad + a_2 C\theta_1 + d_4 S\theta_1 + a_4 C\theta_1 C\theta_2 + d_3 C\theta_1 S\theta_2 - y_7 C\theta_1 S\theta_2 - o_x, \end{aligned} \tag{25}$$

$$\begin{aligned} E_y &= (d_6 - d_5)(C\theta_1 S\theta_4 + C\theta_2 C\theta_4 S\theta_1) + x_7(C\theta_1 C\theta_4 - C\theta_2 S\theta_1 S\theta_4) \\ &\quad - z_7(C\theta_1 S\theta_4 + C\theta_2 C\theta_4 S\theta_1) + d_4 C\theta_1 - a_2 S\theta_1 - a_4 C\theta_2 S\theta_1 - d_3 S\theta_1 S\theta_2 + y_7 S\theta_1 S\theta_2 - o_y, \end{aligned} \tag{26}$$

$$E_z = y_7 C\theta_2 - d_3 C\theta_2 + a_4 S\theta_2 - (d_6 - d_5) C\theta_4 S\theta_2 + z_7 C\theta_4 S\theta_2 + x_7 S\theta_2 S\theta_4 - o_z. \tag{27}$$

The position error function can be defined as

$$J_{pos} = E_x^2 + E_y^2 + E_z^2. \tag{28}$$

By substituting Eqs. (23) and (24) into Eq. (28), it can be seen that J_{pos} is a function of joint variables $\theta_1, \theta_2, \theta_4$ only.

https://doi.org/10.1017/S0263574714001350 Published online by Cambridge University Press

Table I. Identified kinematic parameters of the circumferential drilling machine.

Parameter name	Identified value
a_2	2509.819 mm
α_2	-0.468°
α_3	0.499°
β_3	-0.117°
a_4	199.305 mm
d_4	7.294 mm
α_4	-0.033°
β_4	-0.179°
α_5	-0.056°
β_5	0.200°
α_6	-0.061°
β_6	0.121°
x_7	99.999 mm
y_7	0.233 mm
z_7	−408.968 mm

Since only the Z-axis direction is important in drilling, the orientation objective function is defined by using the faithful geodesic distance as

$$J_{ori} = (C\theta_1 C\theta_2 C\theta_4 - S\theta_1 S\theta_4 - w_x)^2 + (-C\theta_1 S\theta_4 - C\theta_2 C\theta_4 S\theta_1 - w_y)^2 + (C\theta_4 S\theta_2 - w_z)^2, \tag{29}$$

where $S(\bullet)$ and $C(\bullet)$ are sine and cosine functions, respectively, $\theta_1, \theta_2, \theta_4$ are revolute joint variables, and $[w_x, w_y, w_z]^T$ is a unit vector representing the desired Z-axis direction.

The objective function for the inverse kinematics problem is defined as

$$J = \omega_1 J_{\text{ori}} + \omega_2 J_{\text{pos}}. \tag{30}$$

By minimizing the objective function J, joint coordinates for $\theta_1, \theta_2, \theta_4$ can be found. After that, d_3 and $d_6 - d_5$ can be determined in closed-form as shown in Eqs. (23) and (24).

6. Experiments

6.1. Numerical experiments with the nominal model

In the nominal model, parameters $\alpha_2, \alpha_3, \beta_3, \alpha_4, \beta_4, \alpha_5, \beta_5, \alpha_6, \beta_6$ are set to zero, and parameters $a_2, a_4, d_4, x_7, y_7, z_7$ use values from kinematic calibration (refer to Table I).

In the experiments, suitable values for the weights ω_1, ω_2 in Eq. (30) should be assigned. Since the orientation errors evaluated with the faithful geodesic distance function are in the unit of radian and position errors evaluated with the Euclidean distance are in the unit of millimeter, to determine the weights for the position error function and orientation error function, we should answer the question: how many radians in orientation error are equally intolerable as one millimeter in position error? This may be answered according to the accuracy requirements of the specific engineering applications.

For example, for the circumferential drilling machine for aircraft assembly in this research, the required position and orientation accuracy of drilled holes are ± 0.5 mm and ± 0.5 degree, respectively. Thus, $\pi/180$ radian in orientation error is equally intolerable as one millimeter in position error, and weights can be set to $\omega_1 = (180/\pi)^2$, $\omega_2 = 1$. When this kind of engineering information is not available, weighting of the position error and orientation error becomes a matter of choice, and the weights can be simplify set to $\omega_1 = \omega_2 = 1$.

Since prismatic joint variables are not involved in the optimization process, only initial values for the revolute joint variables $\theta_1, \theta_2, \theta_4$ should be provided to start the optimization. For the

https://doi.org/10.1017/S0263574714001350 Published online by Cambridge University Press

Table II. Motion range of the machine joints.

Joint index	Joint type	Range
1	Revolute	$-36^\circ \sim 36^\circ$
2	Revolute	$-5^\circ \sim 5^\circ$
3	Prismatic	$-205 \sim 205$ mm
4	Revolute	$-10^\circ \sim 10^\circ$
5	Prismatic	$-190 \sim 190$ mm
6	Prismatic	$-265 \sim 265$ mm

circumferential drilling machine, the motion range of the revolute joints is relatively small (refer to Table II), hence the initial values can be set to $\theta_1 = \theta_2 = \theta_4 = 0$. The convergence criteria for nonlinear optimization are defined as: minimum variation on joint parameters $TolX = 10^{-8}$, maximum allowable variation of the objective function $TolFun = 10^{-8}$, maximum number of iterations $MaxIter = 100$. The optimization process stops if any of the three criteria is met.

The procedure to carry out the numerical experiment is as follows:

(1) Randomly choose a set of joint parameters $[\theta_1, \theta_2, d_3, \theta_4, d_5, d_6]$ from the machine's joint space (refer to Table I);
(2) Compute the TCP pose using the joint coordinates $[\theta_1, \theta_2, d_3, \theta_4, d_5, d_6]$ and forward kinematics Eq. (18), and denote it as the homogeneous transformation matrix;

$$T_d = \begin{bmatrix} u_x & v_x & w_x & o_x \\ u_y & v_y & w_y & o_y \\ u_z & v_z & w_z & o_z \\ 0 & 0 & 0 & 1 \end{bmatrix}.$$

(3) Take $[w_x, w_y, w_z]^T$ and $[o_x, o_y, o_z]^T$ as the desired orientation and position of the tool axis;
(4) Find the revolute joint coordinates $\theta_1^*, \theta_2^*, \theta_4^*$ to the inverse kinematics problem by minimizing Eq. (30) with the Levenberg–Marquardt nonlinear optimization method. And then find the prismatic joint coordinates with Eqs. (23) and (24)

$$[\theta_1^*, \theta_2^*, d_3^*, \theta_4^*, d_6^* - d_5^*].$$

(5) Calculate the error vector of the joint coordinates found by the algorithm

$$[\Delta_1, \Delta_2, \Delta_3, \Delta_4, \Delta_5] = [\theta_1^* - \theta_1, \theta_2^* - \theta_2, d_3^* - d_3, \theta_4^* - \theta_4, d_6^* - d_5^* - (d_6 - d_5)]. \quad (31)$$

For convenience, the Euclidean norm of this vector can be used as an index to evaluate the accuracy of the proposed method.

Figure 8 shows the results of 10,000 random tests performed on a personal computer (2.0 GHz CPU, 4 GB memory). The maximum error of the found solution is below 1.35×10^{-7}, average running time is 8 ms. The experiments show that both weighting methods lead to similar results.

As a comparison, numerical experiments have also been conducted with the orientation error function defined according to literature[8,34]

$$J_{ori} = ((C\theta_1 C\theta_2 C\theta_4 - S\theta_1 S\theta_4)w_x + (-C\theta_1 S\theta_4 - C\theta_2 C\theta_4 S\theta_1)w_y + (C\theta_4 S\theta_2)w_z - 1)^2. \quad (32)$$

Different weights for the objective function have been tried, and the results are shown in Fig. 9. Although the average running time is comparable to the results obtained with the proposed method, none of these experiments generate accurate solutions to the inverse kinematics problem. Therefore, it can be concluded that orientation error functions like Eq. (32) should be avoided in the formulation of the objective function for solving inverse kinematics problems.

https://doi.org/10.1017/S0263574714001350 Published online by Cambridge University Press

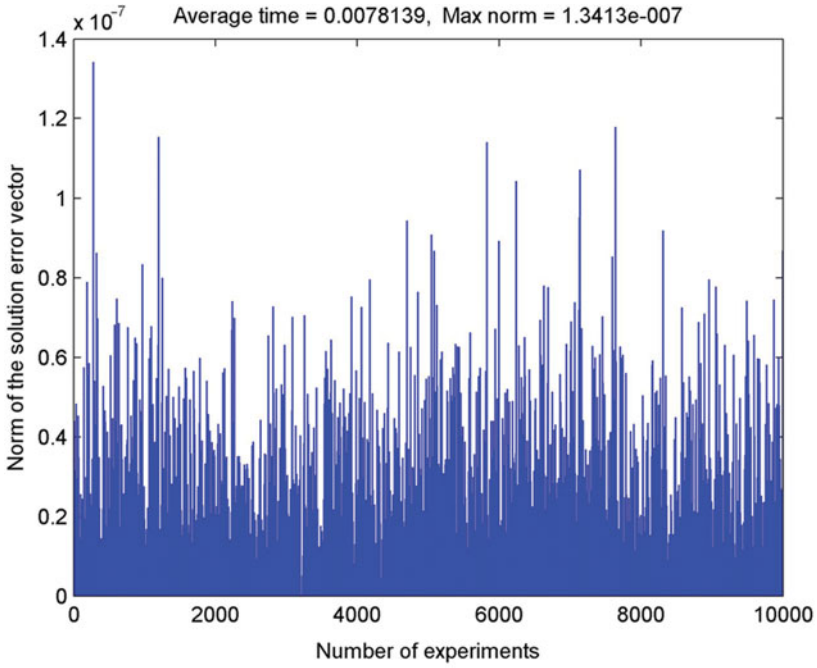

(a)

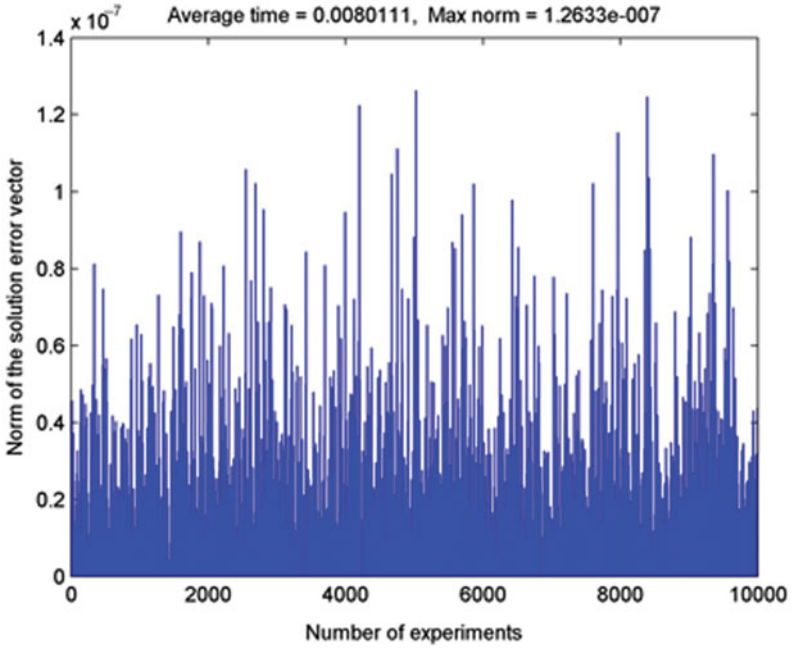

(b)

Fig. 8. Numerical experiments in which the orientation error function (Eq. (29)) is defined with faithful geodesic distance. (a) $\omega_1 = \omega_2 = 1$; (b) $\omega_1 = (180/\pi)^2$, $\omega_2 = 1$; (c) $\omega_1 = 10^4$, $\omega_2 = 1$; (d) $\omega_1 = 10^8$, $\omega_2 = 1$.

6.2. Numerical experiments with the identified kinematic model

In order to achieve high positioning accuracy, manufacturing and assembly errors of the machine need to be considered. In this case, all kinematic parameters should use values obtained from kinematic calibration of the machine (refer to Table I). In this case, partially closed-form solution of the inverse kinematics problem is no longer possible, and all joint coordinates should be identified with nonlinear

https://doi.org/10.1017/S0263574714001350 Published online by Cambridge University Press

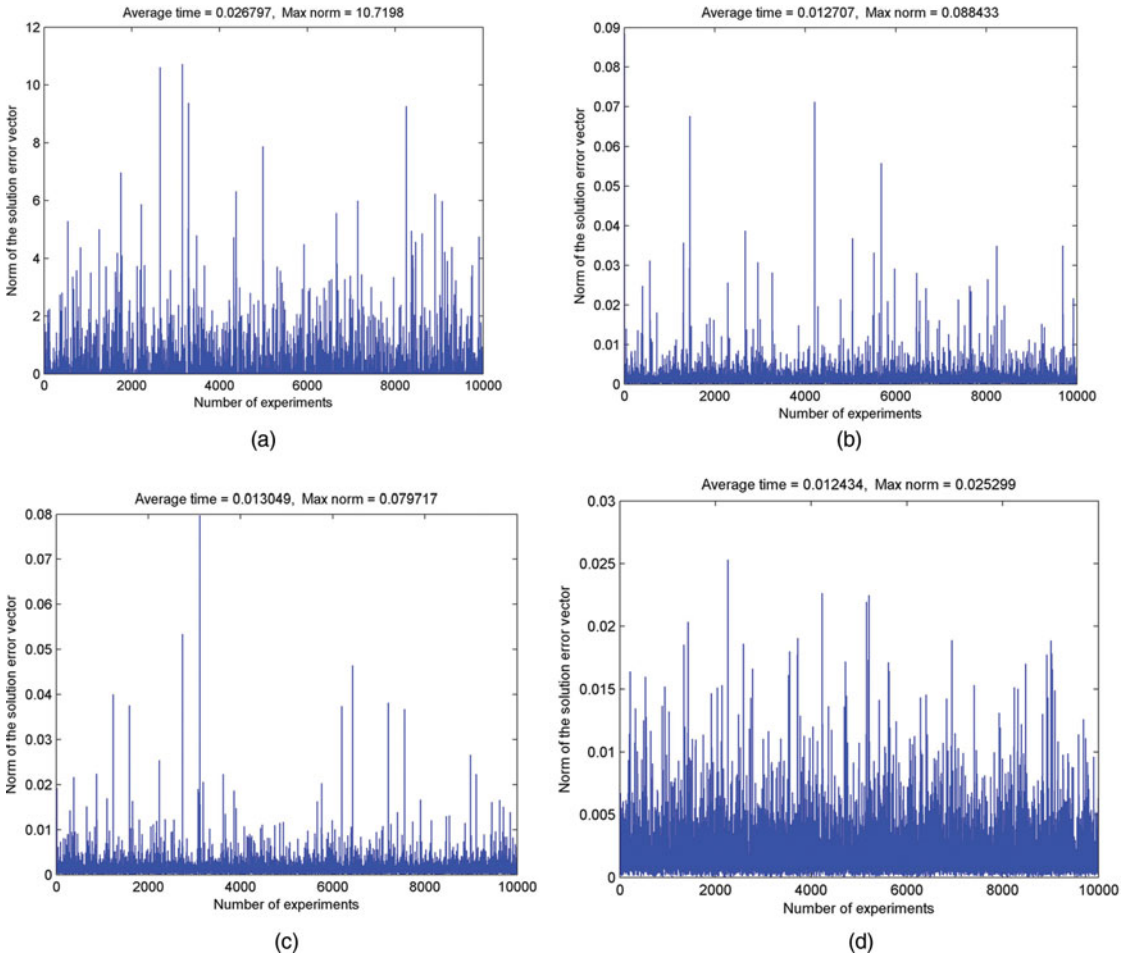

Fig. 9. Numerical experiments in which the orientation error function (Eq. (32)) is defined as in literature.[8,34] (a) $\omega_1 = \omega_2 = 1$; (b) $\omega_1 = (180/\pi)^2$, $\omega_2 = 1$.

optimization. However, the inverse kinematic solution to the nominal inverse kinematics model is still very important, because it can be used as good initial values for nonlinear optimization in solving the inverse kinematics of the identified kinematic model. Ten thousand random experiments have been performed, and the results are shown in Fig. 10. It can be seen that both weighting methods lead to similar results. Average run time is less than 20 ms, and the largest Euclidean norm of the solution vector is less than 2×10^{-4}, which suggests that the inverse kinematic solver meets the speed and accuracy requirement for position control of the circumferential drilling machine.

6.3. Drilling experiments of the circumferential drilling machine

The proposed inverse kinematics algorithm has been integrated into the control system of the circumferential drilling machine, as shown in Fig. 11. Actual drilling experiments have been performed at different quadrants on simulated fuselage sections. The automated drilling process was controlled with NC programs generated in an off-line programming environment, in which the path of the drilling tool is described with position and orientation information in the machine's Cartesian space. Figure 12 shows the experimental system and drilled holes at the top quadrant of the simulated fuselage section. The position errors of the drilled holes with respect to the predefined reference holes were checked with a caliper and were found to be within ± 0.5 mm, which is acceptable according to the accuracy requirement for fastener holes of large aircrafts.

https://doi.org/10.1017/S0263574714001350 Published online by Cambridge University Press

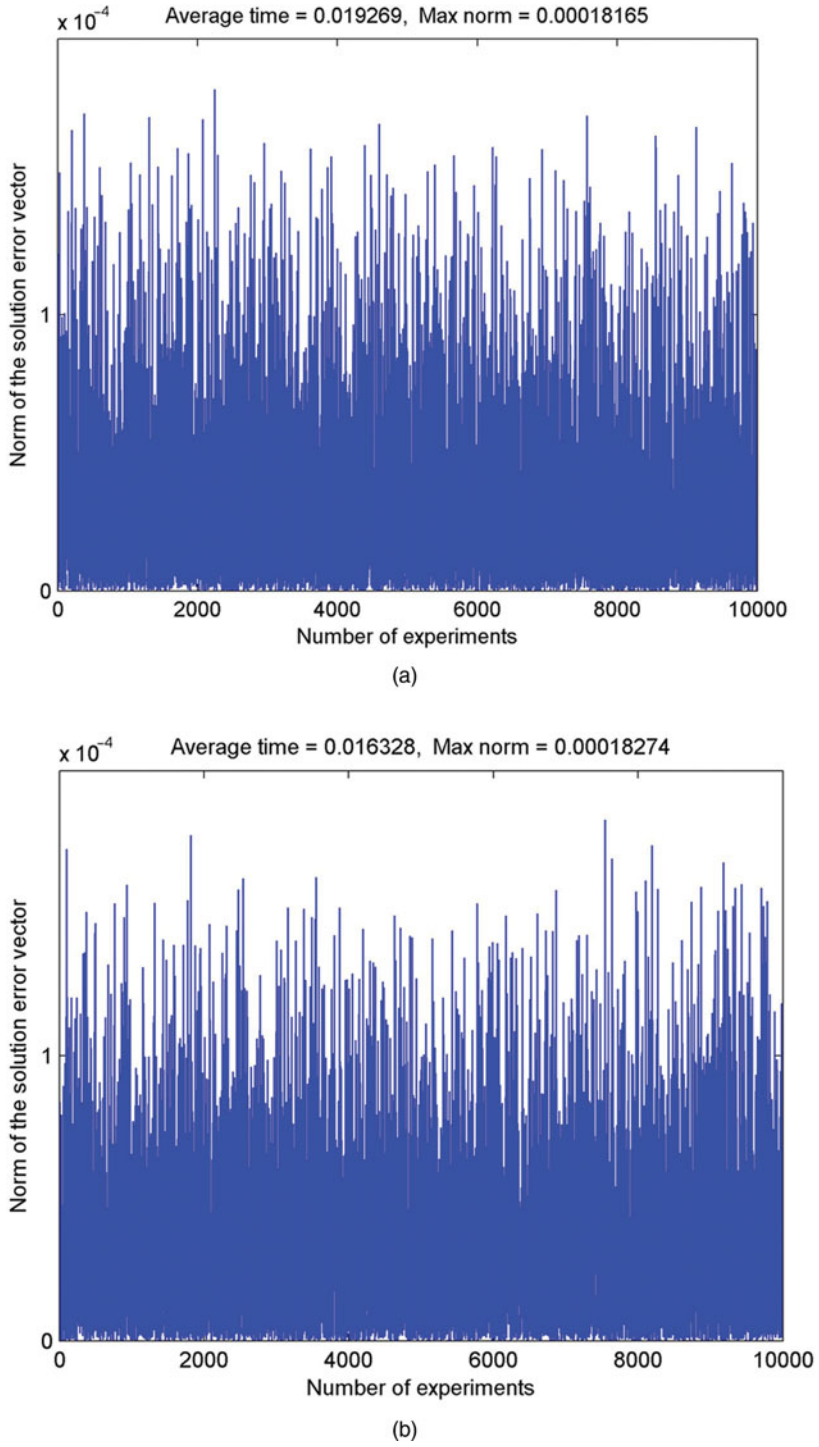

Fig. 10. Numerical experiments with the identified kinematic model. (a) Control software of the circumferential drilling machine; (b) Control system structure of the circumferential drilling machine

7. Conclusions

In this paper, an efficient and robust inverse kinematics algorithm has been proposed for a new circumferential drilling machine for aircraft fuselage assembly. The forward kinematic model of the drilling machine is developed by combining the Denavit–Hartenberg and modified Hayati methods. The inverse kinematics problem is formulated as a nonlinear minimization problem. The faithful geodesic distance function has been proposed to represent the orientation part of the objective function.

https://doi.org/10.1017/S0263574714001350 Published online by Cambridge University Press

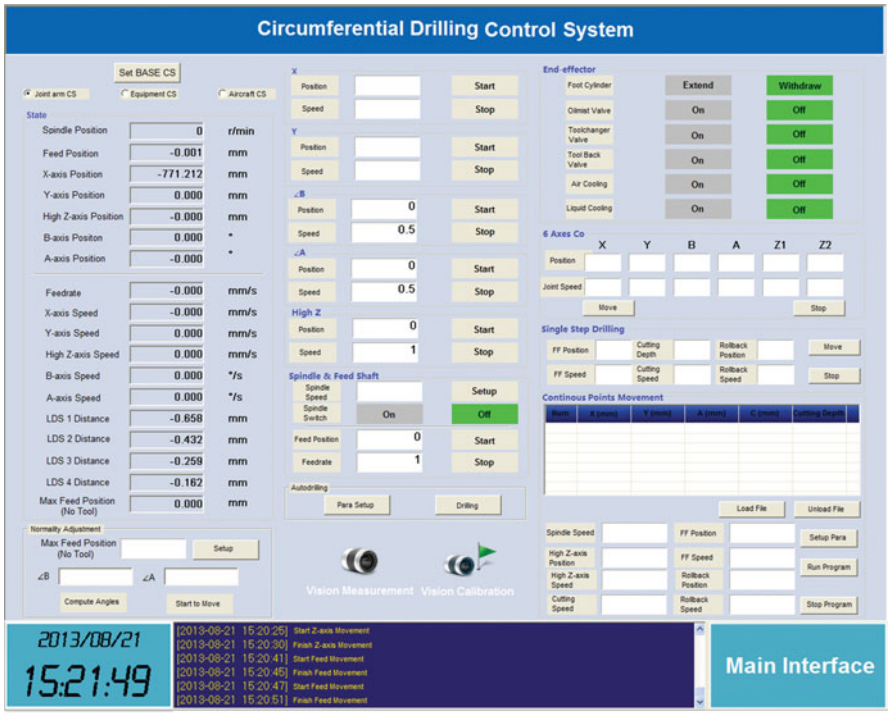

(a)

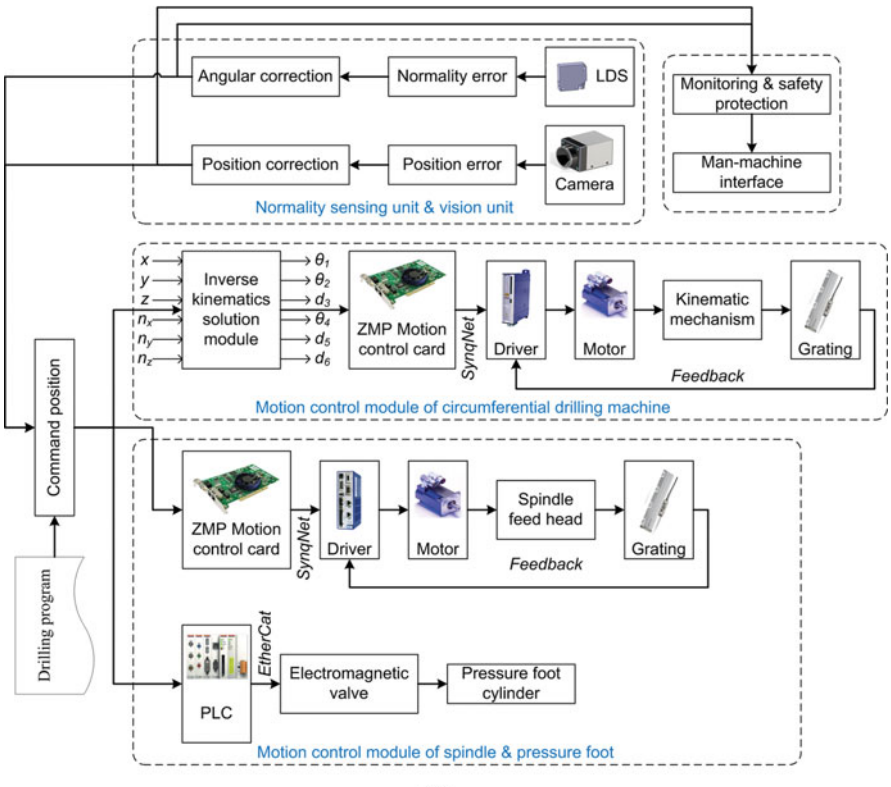

(b)

Fig. 11. Control system of the circumferential drilling machine.

https://doi.org/10.1017/S0263574714001350 Published online by Cambridge University Press

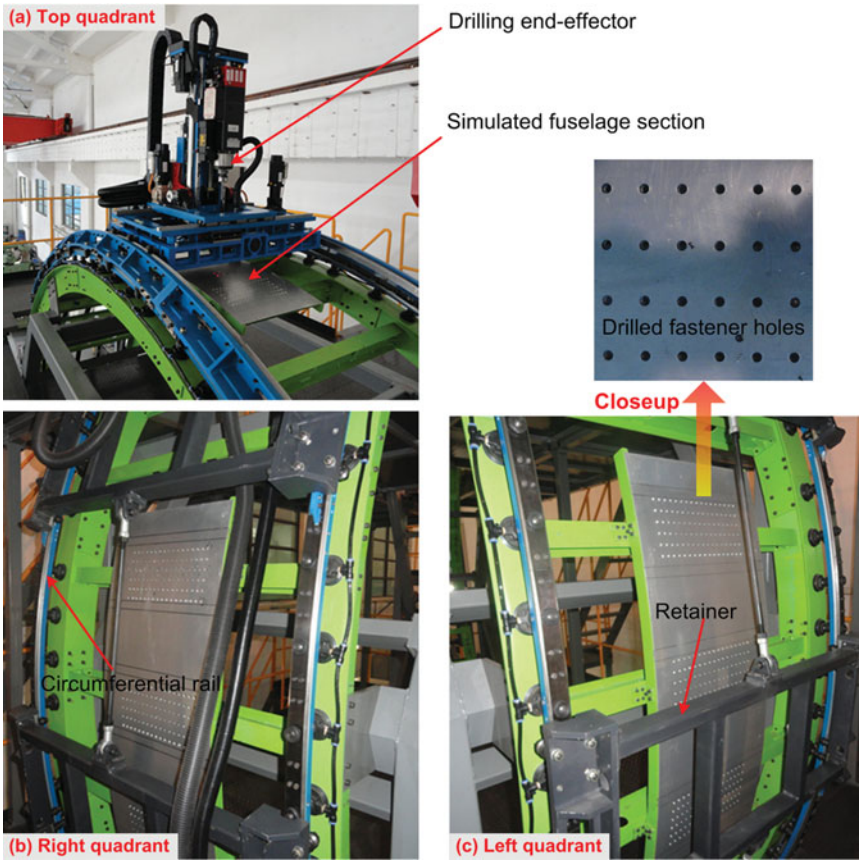

Fig. 12. Drilling experiments performed at different quadrants on simulated fuselage sections.

Theoretical analysis and numerical experiments suggest that orientation error functions formulated with faithful geodesic distance functions have better performance in solving the inverse kinematics problem. Compared with the orientation error functions in literature, the proposed orientation error function defined with faithful geodesic distance is more effective, which leads to more accurate solutions to the inverse kinematics problem. The inverse kinematic problem is decomposed into two subproblems by exploring the characteristics of the circumferential drilling machine. The revolute joint coordinates are found by solving one subsystem with nonlinear optimization, and the prismatic joint coordinates are calculated with closed-form formulas. When the manufacturing and assembly errors of the machine are significant, a partially closed-form solution of the inverse kinematics problem is no longer possible. However, the proposed method can be used to acquire good initial guesses for nonlinear optimization in solving the inverse kinematic problem. Numerical experiments of the proposed algorithm show that when the faithful geodesic distance function is used in formulating the orientation error function, accurate inverse kinematic solutions can be obtained regardless of the weighting methods. The proposed algorithm has been integrated into the control system of the circumferential drilling system, which was successfully used to control the position and orientation of the drill in the machine's workspace. Drilling experiments show that position accuracy of drilled holes is within ± 0.5 mm, which is acceptable for the assembly of large aircrafts.

Acknowledgements

This research was supported by the National Natural Science Foundation of China (Project No. 51205352) and Science Fund for Creative Research Groups of the National Natural Science Foundation of China (Project No.51221004).

References

1. G. Williams, E. Chalupa and S. Rahhal, "Automated positioning and alignment systems," *SAE Trans.* **109**, 737–745 (2000).
2. B. Qiu, J. Jiang and Y. Ke, "A new principle and device for large aircraft components gaining accurate support by ball joint," *J. Zhejiang Univ.-Sci. A* **12**, 405–414 (2011).
3. P. Thompson, H. Oberoi and A. Draper, "Development of a multi spindle flexible drilling system for circumferential splice drilling applications on the 777 airplane," SAE Technical Paper 2008-01-2298, 2008, doi:10.4271/2008-01-2298.
4. H. Oberoi, A. Draper and P. Thompson, "Production implementation of a multi spindle flexible drilling system for circumferential splice drilling applications on the 777airplane," SAE Technical Paper 2009-01-3090 (2009) doi:10.4271/2009-01-3090.
5. Y. Bestaoui, "An unconstrained optimization approach to the resolution of the inverse kinematic problem of redundant and nonredundant robot manipulators," *Robot. Auton. Syst.* **7**, 37–45 (1991).
6. A. Goldenberg, B. Benhabib and R. Fenton, "A complete generalized solution to the inverse kinematics of robots," *IEEE J. Robot. Autom.* **1**, 14–20 (1985).
7. K. Kazerounian. "On the numerical inverse kinematics of robotic manipulators," *ASME J. Mech. Transm. Autom. Des.* **109**, 8–13 (1987).
8. L.-C.T. Wang and C.C. Chen, "A combined optimization method for solving the inverse kinematics problems of mechanical manipulators," *IEEE Trans. Robot. Autom.* **7**, 489–499 (1991).
9. J. Luh, M. Walker and R. Paul, "Resolved-acceleration control of mechanical manipulators," *IEEE Trans. Autom. Control* **25**, 468–474 (1980).
10. E. Freund, "Fast nonlinear control with arbitrary pole-placement for industrial robots and manipulators," *Int. J. Robot. Res.* **1**, 65–78 (1982).
11. R. Manseur and K. L. Doty, "A fast algorithm for inverse kinematic analysis of robot manipulators," *Int. J. Robot. Res.* **7**, 52–63 (1988).
12. D. L. Pieper, The Kinematics of Manipulators Under Computer Control. *Ph.D. dissertation* (Stanford University, Stanford, CA, 1968).
13. M. Raghavan and B. Roth, "Kinematic Analysis of the 6R Manipulator of General Geometry," *Proceedings of the 5th International Symposium on Robotics Research*, MIT Press, Cambridge, MA, USA (1990) pp. 263–269.
14. M. Raghavan and B. Roth, "Solving polynomial systems for the kinematic analysis and synthesis of mechanisms and robot manipulators," *J. Mech. Des.* **117B**, 71–79 (1995).
15. S. Sasaki, "Feasibility studies of kinematics problems in the case of a class of redundant manipulators," *Robotica* **13**, 233–241 (1995).
16. S. Elgazzar, "Efficient kinematic transformations for the PUMA 560 robot," *IEEE J. Robot. Autom.* **1**, 142–151 (1985).
17. J. M. Hollerbach and G. Sahar, "Wrist-partitioned, inverse kinematic accelerations and manipulator dynamics," *Int. J. Robot. Res.* **2**, 61–76 (1983).
18. L.-W. Tsai and A. P. Morgan, "Solving the kinematics of the most general six- and five- degree-of-freedom manipulators by continuation methods," *ASME J. Mech. Trans. Autom. Des.* **107**, 189–200 (1985).
19. R. Ibarra and N. D. Perreira, "Determination of linkage parameter and pair variable errors in open chain kinematic linkages using a minimal set of pose measurement data," *ASME J. Mech. Trans. Autom. Des.* **108**, 159–166 (1986).
20. J. J. Uicker, Jr., J. Denavit and R. S. Hartenberg, "An iterative method for the displacement analysis of spatial mechanisms," *ASME J. Appl. Mech.* **31**, 309–314 (1964).
21. C. W. Wampler, "Manipulator inverse kinematic solutions based on vector formulations and damped least-squares methods," *IEEE Trans. Syst. Man Cybern.* **16**, 93–101 (1986).
22. S. Chiaverini, B. Siciliano and O. Egeland, "Review of the damped least-squares inverse kinematics with experiments on an industrial robot manipulator," *IEEE Trans. Control Syst. Technol.* **2**, 123–134 (1994).
23. Y. Nakamura and H. Hanafusa, "Inverse kinematic solutions with singularity robustness for robot manipulator control," *J. Dyn. Syst. Meas. Control* **108**, 163–171 (1986).
24. K. Levenberg, "A method for the solution of certain non-linear problems in least squares," *Q. Appl. Math* **2**, 164–168 (1944).
25. D. W. Marquardt, "An algorithm for least-squares estimation of nonlinear parameters," *J. Soc. Ind. Appl. Math.* **11**, 431–441 (1963).
26. A. A. Goldenberg and D. L. Lawrence, "A generalized solution to the inverse kinematics of robotic manipulators," *J. Dyn. Syst. Meas. Control* **107**, 103–106 (1985).
27. J. Zhao and N. I. Badler, "Inverse kinematics positioning using nonlinear programming for highly articulated figures," *ACM Trans. Graphics (TOG)* **13**, 313–336 (1994).
28. J. Angeles, "On the numerical solution of the inverse kinematic problem," *Int. J. Robot. Res.* **4**, 21–37 (1985).
29. W. A. Wolovich and H. Elliott, "A Computational Technique for Inverse Kinematics," *Proceedings of the 23rd IEEE Conference on Decision and Control*, vol. 23, pp. 1359–1363 (1984).
30. A. Balestrino, G. de Maria and L. Sciavicco, "Robust Control of Robotic Manipulators," *Proceedings of the 9th IFAC World Congress*, vol. 5, pp. 2435–2440 (1984).

31. T. Sugihara, "Solvability-unconcerned inverse kinematics by the Levenberg–Marquardt method," *IEEE Trans. Robot.* **27**, 984–991 (2011).
32. V. J. Lumelsky, "Iterative coordinate transformation procedure for one class of robots," *IEEE Trans. Syst. Man Cybern.* **SMC-14**, 500–505 (1984).
33. R. Featherstone, "Position and velocity transformations between robot end-effector coordinates and joint angles," *Int. J. Robot. Res.* **2**, 35–45 (1983).
34. A. S. Deo and I. D. Walker, "Adaptive Non-Linear Least Squares for Inverse Kinematics," *Proceedings of IEEE International Conference on Robotics and Automation*, vol. 1, pp. 186–193 (1993).
35. B. Siciliano and O. Khatib, *Springer Handbook of Robotics* (Springer, Berlin, 2008).

https://doi.org/10.1017/S0263574714001350 Published online by Cambridge University Press